Animations and Properties of Three SDOF Damping Systems

Jeng-Tzong Chen[1]; Jia-Wei Lee[2]; Shing-Kai Kao[3]; and Sheng-Kuang Chen[4]

Abstract: Three models—the viscous damping model, the new hysteretic damping model, and the Coulomb damping model—are studied in this paper. For the viscous damping and the Coulomb damping models, the free vibration problem is reviewed and demonstrated by animations. Regarding the new hysteretic damping model, the free vibration problem for the different range of parameters, namely $0 < \eta < 1$, $\eta = 1$, and $\eta > 1$ are analytically derived and are also demonstrated by animations. In particular, the exact solutions of the latter two cases are derived for the first time. In animations, the trajectories for three damping models in the phase plane consist of straight lines, quarter ellipses, and hyperbolic curves. For the case of $\eta \geq 1$, it is interesting that permanent deformation may occur. In addition, the dead zone for the Coulomb damping model in the phase plane is also addressed. The envelope for the amplitude decay yields exponential, geometric, and linear curves for the viscous damping model, the new hysteretic damping model and the Coulomb damping model, respectively. It is also the primary focus that the same period and the same ratio of amplitude decay for the relation between the viscous coefficient and the hysteretic parameter are constructed. All animations are produced using the symbolic software Mathematica because it is easy for readers to understand the physical behavior of three damping models. **DOI: 10.1061/(ASCE)EM.1943-7889.0001481.**

Author keywords: Viscous damping; New hysteretic damping; Coulomb damping; Phase plane; Dead zone; Ratio of amplitude decay.

Introduction

Damping characteristics are often used to suppress the vibration level by using various energy dissipation mechanisms. Three damping models, the viscous damping model, the hysteretic damping model, and the Coulomb damping model, have been discussed in the literature of structural dynamics and viscoelasticity (Meirovitch 1986; Clough and Penzien 1975). In the viscous damping model, the viscous damping force is proportional to the velocity. It opposes the motion through the process (Beards 1995). In the Coulomb damping model, Coulomb damping relates to the friction of the contact surface. It resists a body to slide and causes energy to dissipate (Zhuravlev 2013). For a large variety of materials, experiments show that energy loss is independent on the excitation frequency. This material damping is referred as the hysteretic damping (Beards 1995). The mechanical models for three damping models are shown in Figs. 1(a–c).

[1]Professor, Dept. of Harbor and River Engineering, National Taiwan Ocean Univ., 2 Pei-Ning Rd., Keelung 20224, Taiwan; Professor, Dept. of Mechanical and Mechatronic Engineering, National Taiwan Ocean Univ., 2 Pei-Ning Rd., Keelung 20224, Taiwan (corresponding author). Email: jtchen@mail.ntou.edu.tw

[2]Assistant Professor, Dept. of Civil Engineering, Tamkang Univ., No.151, Yingzhuan Rd., Tamsui Dist., New Taipei City 25137, Taiwan. Email: jwlee@mail.tku.edu.tw

[3]Research Assistant, Dept. of Harbor and River Engineering, National Taiwan Ocean Univ., 2 Pei-Ning Rd., Keelung 20224, Taiwan. Email: m96520009@mail.ntou.edu.tw

[4]Master Student, Dept. of Harbor and River Engineering, National Taiwan Ocean Univ., 2 Pei-Ning Rd., Keelung 20224, Taiwan. Email: 10552026@mail.ntou.edu.tw

Note. This manuscript was submitted on September 20, 2017; approved on January 23, 2018; published online on May 30, 2018. Discussion period open until October 30, 2018; separate discussions must be submitted for individual papers. This paper is part of the ***Journal of Engineering Mechanics***, © ASCE, ISSN 0733-9399.

A great deal of effort on the frequency domain approach simulates the physical phenomenon, e.g., the hysteretic damping model. In the literature (Meirovitch 1986; Nashif et al. 1985), the analogy between viscous and hysteretic damping models have been proposed in the time domain and the frequency domain. Because the frequency domain approach for the hysteretic damping model does not obey the causality condition as pointed out in Sun and Lu (1994), many researchers used the time domain approach to solve this problem. To ensure the causality condition, the model constraint in the frequency domain approach is that the real part and imaginary part of the complex modulus must satisfy the Hilbert transform pair. The related works were proposed by Kelly, Inaudi, and Makris (Inaudi and Kelly 1995; Inaudi and Makris 1996; Makris et al. 1996; Makris 1997), as well as Chen and You (1997, 1999). Chen and You solved the hysteretic damping model by the direct iteration technique and extended to multiple degrees of freedom (MDOF) in the time domain (Chen and You 1997). They primarily employed the fast Fourier transform (FFT) method to solve governing equation in the frequency domain for harmonic loading (Chen and You 1999). The hysteresis loop is constructed to demonstrate that the model in the time domain is fully equivalent to the one in the frequency domain, and the dissipation energy is independent of the exciting frequency.

The free vibration problem for the new hysteretic damping model has been solved (Chen et al. 1994a, b; Caughey and Vijayaraghavan 1970) in the time domain while the loss factor is between zero and one. It is found that the system is nonlinear. Therefore, attention has been paid to the equivalent linearization technique (Beucke and Kelly 1985). In 1994, Chen et al. (1994a) employed the phase plane method for the free vibration of the new hysteretic damping model in the time domain. Although the model in Chen et al. (1994a) satisfies the causality condition, Crandall (1995) criticized that the model is not fully equivalent to the hysteretic damping model of the original problem in the frequency domain. We cannot obtain the complex stiffness $k(1 + i\eta)$ by taking the Fourier transform. Thus, Crandall termed it a new

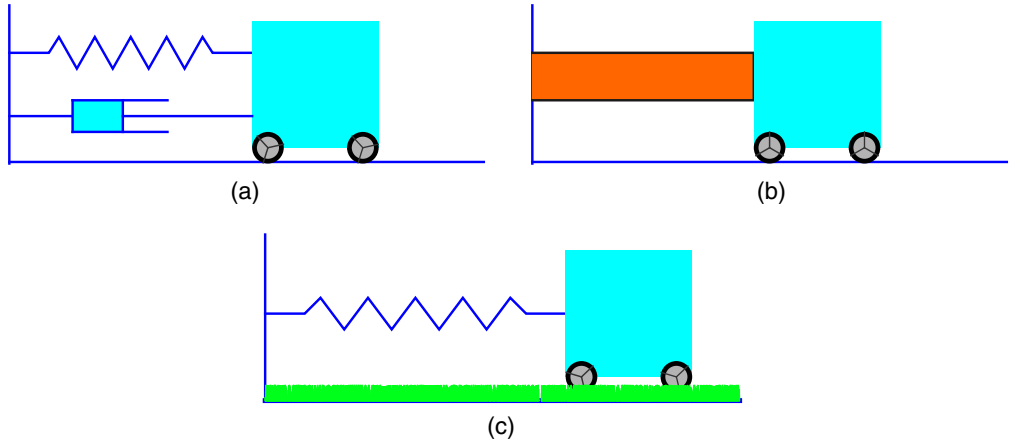

Fig. 1. Mechanical systems of three damping models: (a) viscous damping model; (b) new hysteretic damping model; and (c) Coulomb damping model.

hysteretic damping model. In 1999, Kuo and Chen (1999) further solved an analytical solution for the forced vibration of single degree of freedom with a new hysteretic damping model in the time domain.

The computational tools of symbolic software such as Mathematica, Reduce, Macsyma, and Maple were employed to simulate free vibration and force vibration problems as numerical experiments for a string with spring, mass and damper. Chen et al. (2009) have used Mathematica to solve a series of animations about 1D wave phenomenon.

In this paper, we first revisited analytical solutions for the free vibration problem of three damping models in the time domain. Second, we employed the symbolic software, Mathematica to make corresponding animations. To compare with two damping models confined to power law decay envelopes, the same period and the same ratio of the amplitude decay in the viscous damping model and the new hysteretic model are two indices for the analogy. To have the same damped period, the relation between the viscous coefficient and hysteretic parameter is constructed. In addition, the relation between the viscous coefficient and hysteretic parameter is also utilized in order to have the same ratio of amplitude decay. In the phase plane, trajectories of three damping models are plotted by using the symbolic software, Mathematica, in detail.

Also, there are two focuses except the animation of the three damping models. To the best of authors' knowledge, for the two cases of $\eta = 1$ and $\eta > 1$ for the new hysteretic damping model, the exact solutions are derived for the first time. The second one is to construct the same period and the same ratio of amplitude decay for the relation between the viscous coefficient and the hysteretic parameter. In addition, all numerical results such as the behavior of the amplitude decay can be for reference to choose the proper damping model in the experiment. From an educational point of view, once students obtain the experimental data of decay behavior (linear, exponential, or geometric), they can choose the corresponding Coulomb damping, viscous damping, or hysteretic damping. Therefore, a black box becomes apparent to be three damping models by more physical meaning. The goal is to help students understand the physical phenomenon of damping models better.

Formulation of Three Damping Models

In the viewpoint of civil engineering education, a viscous damping model, a new hysteretic damping model, and a Coulomb damping model are very common in engineering practice and easy to understand for students. These three damping models are very classical elements in simplifying and simulating engineering problems. We employed the single degree of the freedom (SDOF) system to introduce the physical behavior of three damping models. The present hysteric damping is different with the conventional one, so we call it a new hysteric damping. Three mathematical models are explained in the following subsections.

Viscous Damping Model

The most popular damping model is the viscous damping (Meirovitch 1986; Clough and Penzien 1975). The governing equation in the time domain of the single degree of freedom system is

$$m\ddot{x}(t) + c\dot{x}(t) + kx(t) = Pe^{i\omega t} \tag{1}$$

where c = damping coefficient of a viscous damping; m = mass; k = stiffness; $x(t)$ = displacement at time t; and P = amplitude of a harmonic force with the frequency ω. In the case of free vibration, Eq. (1) can be reduced as

$$\ddot{x}(t) + 2\xi\omega_n\dot{x}(t) + \omega_n^2 x(t) = 0 \tag{2}$$

where ξ is the damping ratio as $\xi = c/(2\sqrt{mk})$; and ω_n is the natural frequency of the undamped system as $\omega_n = \sqrt{k/m}$. For the specific initial displacement x_0 and initial velocity $\dot{x}_0$, the solutions of Eq. (2) for the different range of the damping ratio are

Case (a) $\xi > 1$

$$x(t) = \left(x_0\cosh(\omega_v t) + \frac{\dot{x}_0 + \xi\omega_n x_0}{\omega_v}\sinh(\omega_v t)\right)e^{-\xi\omega_n t} \tag{3}$$

Case (b) $\xi = 1$

$$x(t) = ((\dot{x}_0 + \xi\omega_n x_0)t + x_0)e^{-\xi\omega_n t} \tag{4}$$

Case (c) $\xi < 1$

$$x(t) = \left(x_0\cos(\omega_v t) + \frac{\dot{x}_0 + \xi\omega_n x_0}{\omega_v}\sin(\omega_v t)\right)e^{-\xi\omega_n t} \tag{5}$$

where the damped frequency ω_v is

$$\omega_v = \omega_n \sqrt{|1-\xi^2|} \tag{6}$$

According to the damping ratio, the viscous damping is classified into overdamped ($\xi > 1$), critical damped ($\xi = 1$), and underdamped ($\xi < 1$). When $\xi > 1$, there are two different real roots. There is a double real root for $\xi = 1$. For the case of $\xi < 1$, the roots are complex conjugate. In this case, it oscillates near the equilibrium position with the amplitude gradually decreasing to zero. The value of the viscous damping ratio $\xi = 1$ is the critical value that can be used to determine whether the viscous damping system oscillates or not.

Fig. 2 further explains how to determine the trajectories across the quadrant by displacement and velocity functions in the phase plane. For the case of $\xi < 1$, the dimensionless damped period is found to be

$$\frac{T_v}{T_n} = \frac{2\pi/\omega_v}{2\pi/\omega_n} = \frac{1}{\sqrt{1-\xi^2}} \tag{7}$$

where T_ν = period of a viscous damping; and T_n = period of the undamped system. The ratio of amplitude decay is

$$R_v = \frac{A_{k+1}^v}{A_k^v} = e^{-\xi\omega_n T_v} = e^{-2\xi\pi/\sqrt{1-\xi^2}}, \quad k = 0, 1, 2, \ldots \tag{8}$$

where A_k^v = amplitude for the viscous damping in the kth cycle response as shown in Fig. 2; and A_0^v = initial amplitude in the

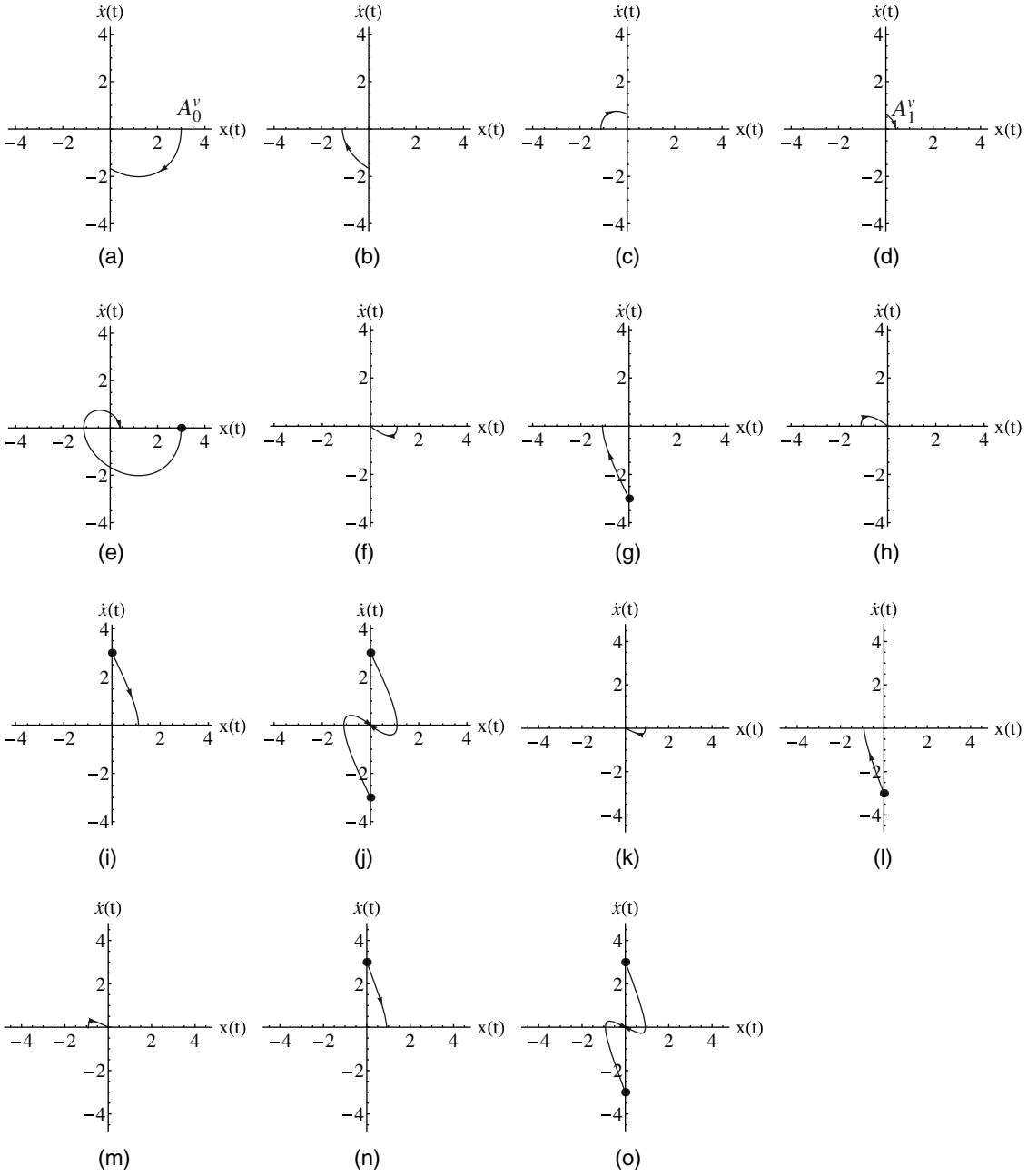

Fig. 2. Trajectories of the phase plane for the viscous damping model, $\omega_v = \omega_n\sqrt{|1-\xi^2|}$: (a) Quadrant IV, $\xi < 1$; (b) Quadrant III, $\xi < 1$; (c) Quadrant II, $\xi < 1$; (d) Quadrant I, $\xi < 1$; (e) the total solution for $\xi < 1$; (f) Quadrant IV, $\xi = 1$; (g) Quadrant III, $\xi = 1$; (h) Quadrant II, $\xi = 1$; (i) Quadrant I, $\xi = 1$; (j) the total solution for $\xi = 1$; (k) Quadrant IV, $\xi > 1$; (l) Quadrant III, $\xi > 1$; (m) Quadrant II, $\xi > 1$; (n) Quadrant I, $\xi > 1$; and (o) the total solution for $\xi > 1$.

J. Eng. Mech., 2018, 144(8): 04018062

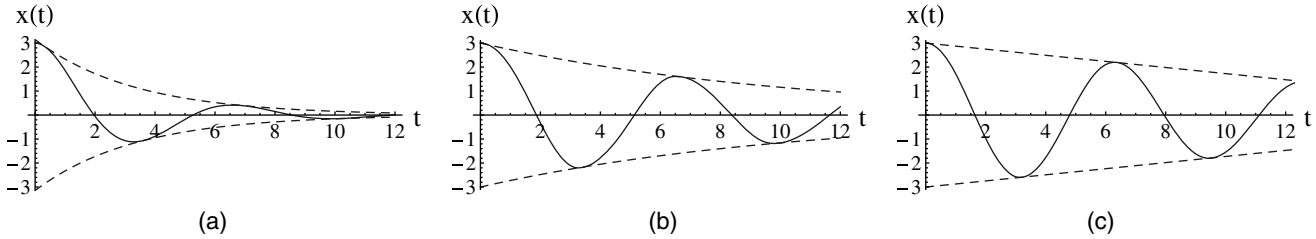

Fig. 3. Displacement history for three damping models: (a) exponential decay for the viscous damping; (b) geometric decay for the new hysteretic damping; and (c) linear decay for the Coulomb damping.

phase plane. The series of A_k^v shows an exponential decay sequence as given in Fig. 3(a) The envelope function $Z_k(t)$ of each maximum response is

$$Z_v(t) = A_1^v e^{-\xi\omega_n(t-T_1^v)} \tag{9}$$

where T_1^v is the time of maximum response when A_1^v occurs.

Hysteretic Damping Model

The governing equation of single degree of freedom for hysteretic damping model was formulated as (Meirovitch 1986)

$$m\ddot{x}(t) + \frac{h}{\omega}\dot{x}(t) + kx(t) = p(t) \tag{10}$$

where h = hysteretic damping coefficient; and $p(t)$ = harmonic force with the frequency ω. To make the transfer functions conjugate for $-\omega$ and ω, the governing equation was further modified to be

$$m\ddot{x}(t) + \frac{h}{|\omega|}\dot{x}(t) + kx(t) = p(t) \tag{11}$$

Because the force term $p(t)$ vanishes when we consider the condition of free vibration, Eq. (11) is ambiguous due to the presence of force frequency $|\omega|$ in the denominator. On the frequency domain, the hysteretic damping model from Eq. (11) can be taking the Fourier transform as (Gaul et al. 1985; Gaul 1989)

$$-m\omega^2\bar{X}(\omega) + k(1 + \text{sgn}(\omega)i\eta)\bar{X}(\omega) = \bar{P}(\omega) \tag{12}$$

where $\bar{X}(\omega)$ = displacement in the frequency domain; the term $k(1 + \text{sgn}(\omega)i\eta)$ is a complex-valued stiffness; the loss factor $\eta = h/k$; and the $\text{sgn}(\omega)$ is 1 when $\omega > 0$ and -1 when $\omega < 0$. Chen and You (1997, 1999) and Inaudi and Kelly (1995) took the inverse Fourier transform for Eq. (12), the governing equation has been derived as shown

$$m\ddot{x}(t) - \frac{k\eta}{\pi}\int_{-\infty}^{\infty}\frac{x(u)}{t-u}du + kx(t) = p(t) \tag{13}$$

with the initial conditions at $t = -\infty$ being

$$x(t)|_{t=-\infty} = 0, \qquad \dot{x}(t)|_{t=-\infty} = 0 \tag{14}$$

In the case of free vibration, $p(t) = 0$, the envelope of decay function $Z_h^o(t)$ is

$$Z_h^o(t) = \left(\frac{1-(2\pi/\eta)}{1+(2\pi/\eta)}\right)^{\frac{t}{T_h^o}} \tag{15}$$

where T_h^o = period of the hysteretic damping.

Rather than solving the hysteretic damping model from Eq. (11) for the problem of free vibration, it is more reasonable for the free vibration solution $x(t)$ from Eq. (13) if the $p(t)$ vanishes in the time domain. The term of causality is defined as the effect (response) does not precede cause (excitation) by Makris (1997). Chen and You (1997, 1999) compared the history of harmonic force and displacement of response in the time domain and frequency domain, respectively. Both of the results showed that the displacement was reacted slightly before the hysteretic damping model under the harmonic force. For the forced vibration, this numerical result of the hysteretic damping model does not obey the natural phenomenon, therefore Chen and You (1997, 1999) called it noncasual effect.

New Hysteretic Damping Model

In the case of free vibration (Chen et al. 1994a), the governing equation for a new hysteretic damping of the single degree of freedom system in the time domain can be written as

$$\ddot{x}(t) + \eta\omega_n^2\frac{|x(t)|}{|\dot{x}(t)|}\dot{x}(t) + \omega_n^2 x(t) = 0 \tag{16}$$

By setting the initial state $(x_0, \dot{x}_0)$, we obtain the solution of Eq. (16) by using the phase plane method in the different range of the loss factor as shown

Case (a): $\eta > 1$

$$x(t) = \begin{cases} x_0\cos(\omega_{h1}t) + \dfrac{\dot{x}_0}{\omega_{h1}}\sin(\omega_{h1}t), & \text{in the 1st and 3rd quadrants} \\ x_0\cos(\omega_{h2}t) + \dfrac{\dot{x}_0}{\omega_{h2}}\sin(\omega_{h2}t), & \text{in the 2nd and 4th quadrants} \end{cases} \tag{17}$$

Case (b): $\eta = 1$

$$x(t) = \begin{cases} x_0\cos(\omega_{h1}t) + \dfrac{\dot{x}_0}{\omega_{h1}}\sin(\omega_{h1}t), & \text{in the 1st and 3rd quadrants} \\ \dot{x}_0 t + x_0, & \text{in the 2nd and 4th quadrants} \end{cases} \tag{18}$$

Case (c): $\eta < 1$

$$x(t) = \begin{cases} x_0 \cos(\omega_{h1} t) + \dfrac{\dot{x}_0}{\omega_{h1}} \sin(\omega_{h1} t), & \text{in the 1st and 3rd quadrants} \\ x_0 \cos(\omega_{h2} t) + \dfrac{\dot{x}_0}{\omega_{h2}} \sin(\omega_{h2} t), & \text{in the 2nd and 4th quadrants} \end{cases} \tag{19}$$

where the damped frequencies in each quadrant are

$$\omega_{h1} = \omega_n \sqrt{1+\eta}, \quad \text{in the 1st and 3rd quadrants}$$
$$\omega_{h2} = \omega_n \sqrt{1-\eta}, \quad \text{in the 2nd and 4th quadrants} \tag{20}$$

Note that the solution of Cases (a) and (b) are obtained for the first time.

Chen et al. (1994a, b) have studied the trajectories for some cases. Fig. 4 further shows how to determine the trajectories in each quadrant by using the phase plane method. The value of the hysteretic damping loss factor $\eta = 1$ is the critical value that can be used to determine whether the hysteretic damping system oscillates or not. For the case of $\eta < 1$, the dimensionless damped period is

$$\frac{T_h^n}{T_n} = \frac{\sqrt{1+\eta} + \sqrt{1-\eta}}{2\sqrt{1-\eta^2}} \tag{21}$$

where T_h^n = period of the new hysteretic damping. The ratio of amplitude decay is

$$R_h = \frac{A_{k+1}^h}{A_k^h} = \frac{1-\eta}{1+\eta}, \quad k = 0, 1, 2, \ldots \tag{22}$$

where A_k^h means the amplitude for the new hysteretic damping in the kth cycle response as shown in Fig. 4, and A_0^h represents the initial amplitude. The series of A_k^h shows a geometric decay as given in Fig. 3(b). The envelope function $Z_h^n(t)$ of each maximum response is

$$Z_h^n(t) = A_1^h \left(\frac{1-\eta}{1+\eta} \right)^{\frac{(t-T_1^h)}{T_h^n}} \tag{23}$$

where T_1^h is the time of maximum response when A_1^h occurs. The differences of the hysteretic damping model and the new hysteretic damping model from the governing equation, linearity, casuality, envelope of decay, and damping period are shown in Table 1. The symbols of the original hysteretic damping for the envelope of decay and damping period are Z_h^o and T_h^o, and the symbols of the new hysteretic damping are Z_h^n and T_h^n, respectively.

Coulomb Damping Model

The governing equation of the single degree of freedom system with a Coulomb damping (Zhuravlev 2013) in the time domain can be represented as

$$\ddot{x}(t) + \frac{k}{m} x(t) = g\mu_k \frac{\dot{x}(t)}{|\dot{x}(t)|} \tag{24}$$

where μ_k and g are the dynamic friction coefficient and the acceleration of gravity, respectively. Eq. (24) can be transformed into

$$\ddot{x}(t) + \omega_n^2 x(t) = F_d \tag{25}$$

where F_d relates to the Coulomb friction (Zhuravlev 2013). When the restoring force is smaller than the maximum static friction, a mass becomes rest. Otherwise, the resultant force can drive the mass away. For the relative translational sliding, the resistance force F_d or so called the kinetic friction is defined as

$$\begin{aligned} F_d &= -a\omega_n^2, && \dot{x}(t) > 0 \\ F_d &= a\omega_n^2, && \dot{x}(t) < 0 \\ F_d &\in [-g\mu_s, g\mu_s], && \dot{x}(t) = 0 \end{aligned} \tag{26}$$

where a = friction parameter on the sliding surface; and μ_s = static friction coefficient. We can also obtain the solution of Eq. (25) in each quadrant of the phase plane with the specified initial state $(x_0, \dot{x}_0)$

$$x(t) = \begin{cases} (x_0 + a) \cos(\omega_n t) + \dfrac{\dot{x}_0}{\omega_n} \sin(\omega_n t) - a, & \text{in the 1st and 2nd quadrants} \\ (x_0 - a) \cos(\omega_n t) + \dfrac{\dot{x}_0}{\omega_n} \sin(\omega_n t) + a, & \text{in the 3rd and 4th quadrants} \end{cases} \tag{27}$$

The damped frequency of this model is the same as the natural frequency ω_n. Fig. 5 further shows that the solution of the trajectories in the four quadrants.

The total time to travel through the four quadrants yields the dimensionless damped period as

$$\frac{T_c}{T_n} = 1 \tag{28}$$

where T_c = period of Coulomb damping. It is different from that of the viscous damping and the hysteretic damping. The amplitude decay D_c is

$$D_c = A_{k+1}^c - A_k^c = -4a, \quad k = 0, 1, 2, \ldots \tag{29}$$

where A_k^c means the amplitude for the Coulomb damping in the kth cycle response in Fig. 5; and A_0^c also represents the initial

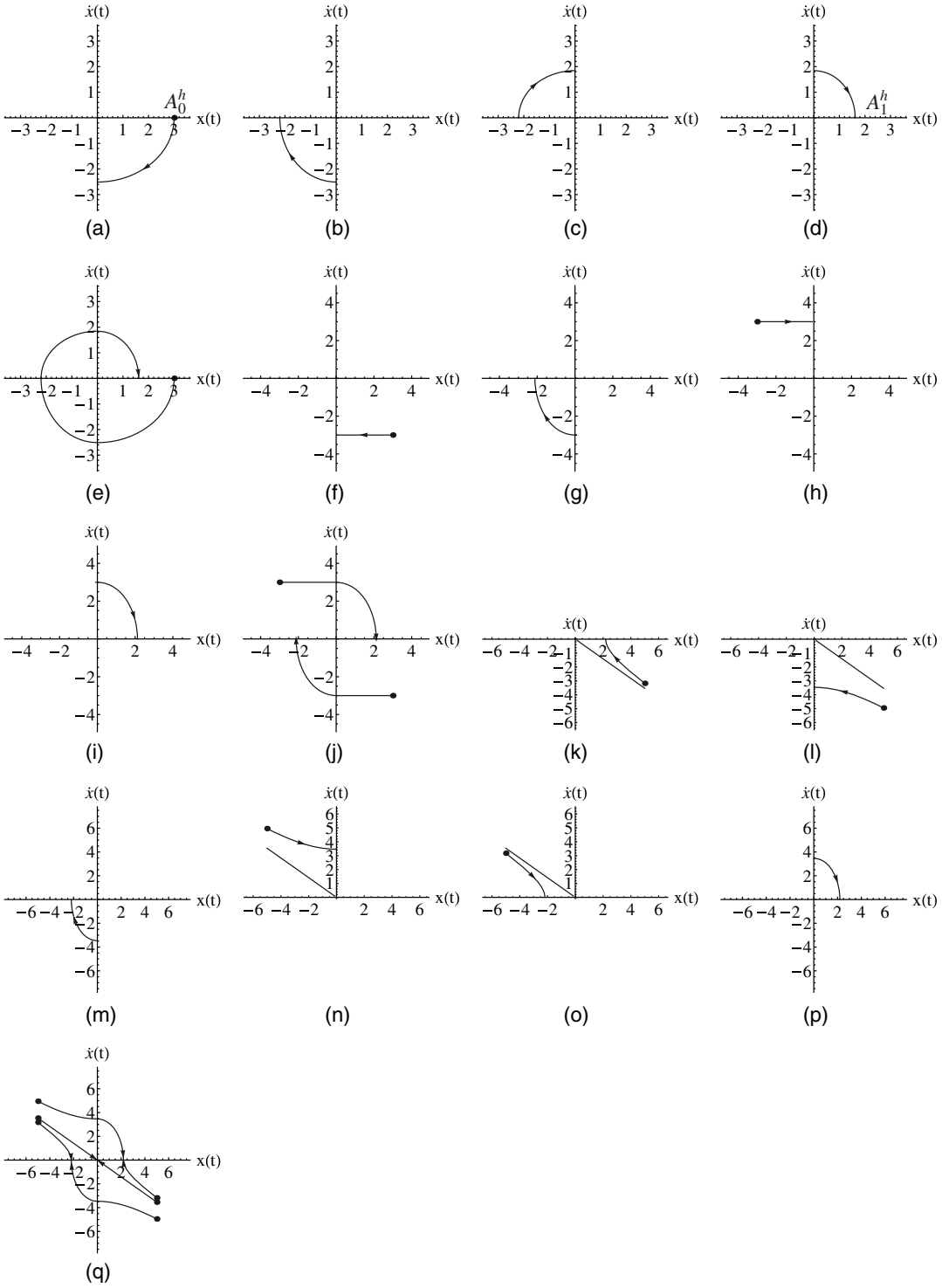

Fig. 4. Trajectories of the phase plane for the new hysteretic damping model, $\omega_{h1} = \omega_n\sqrt{1+\eta}$, $\omega_{h2} = \omega_n\sqrt{1-\eta}$: (a) Quadrant IV, $\eta < 1$; (b) Quadrant III, $\eta < 1$; (c) Quadrant II, $\eta < 1$; (d) Quadrant I, $\eta < 1$; (e) the total solution for $\eta < 1$; (f) Quadrant IV, $\eta = 1$; (g) Quadrant III, $\eta = 1$; (h) Quadrant II, $\eta = 1$; (i) Quadrant I, $\eta = 1$; (j) the total solution for $\eta = 1$; (k) Quadrant IV, $\eta > 1$; (l) Quadrant IV, $\eta > 1$; (m) Quadrant III, $\eta > 1$; (n) Quadrant II, $\eta > 1$; (o) Quadrant II, $\eta > 1$; (p) Quadrant I, $\eta > 1$; and (q) the total solution for $\eta > 1$.

amplitude. The series A_k^c displays a linear decay sequence as shown in Fig. 3(c). The envelope function $Z_c(t)$ of each maximum response is

$$Z_c(t) = A_1^c + \frac{-4a}{T_c}(t - T_1^c) \tag{30}$$

where T_1^c = time of maximum response when A_1^c occurs.

For the case of a viscous damping, it gradually decreases to the origin in the phase plane. Once the restoring force cannot overcome the friction force in the Coulomb damping system, it leads to rest. This range in the x-axis is called the dead zone in the phase plane. For the static equilibrium, the value of a represents the range of the dead zone. It can be derived by using Eqs. (23)–(25) as shown

Table 1. Comparison of the new hysteretic damping and hysteretic damping model

Characteristic	New hysteretic damping model (Chen et al. 1994a)	Hysteretic damping model (Chen and You 1997, 1999)
Governing equation	Eq. (16)	Eq. (13), for $p(t) = 0$
Form of equation	Ordinary-differential equation	Integral-differential equation
Linearity	Nonlinear	Linear
Casuality	Obey casual effect	Do not obey casual effect
Envelope of decay	Eq. (23)	Eq. (15)
Damping period	Eq. (21)	T_h^o is not applicable

$$-a\omega_n^2 = -g\mu_k \le \frac{k}{m}x(t) \le g\mu_k = a\omega_n^2 \tag{31}$$

The dead zone locates on the interval of $-a \le x \le a$ along the x-axis.

Illustrative Examples with Animation Using the Mathematica

According to the aforementioned formulation, trajectories in the phase plane of three damping models for various initial conditions are discussed in detail in this section. The natural frequency ω_n for the three systems is set to be 1 rad per second for simplicity.

Viscous Damping Model

For the viscous damping model, all possible initial states $(x_0, \dot{x}_0)$ are summarized in Table 2. In the case of overdamping ($\xi > 1$) model, the damping ratio of viscous damping is $\xi = 1.5$. Figs. 6(a and b) show the trajectories in the phase plane for the cases of overdamping and critical damping. It is found that trajectories shrink to the origin very quickly. For the underdamped case ($\xi = 0.3$), the trajectories in the phase plane for various initial states are shown in Fig. 6(c). In this situation, spiral trajectories shrink to the origin.

Table 2. Initial state $(x_0, \dot{x}_0)$ of viscous damping

Case number	$(x_0, \dot{x}_0)$
$\xi > 1$ ($\xi = 1.5$)	
a1	(3, 0)
a2	$(3, -3)$
a3	$(0, -3)$
a4	$(-3, -3)$
a5	$(-3, 0)$
a6	$(-3, 3)$
a7	(0, 3)
a8	(3, 3)
$\xi = 1$	
b1	(3, 0)
b2	$(3, -3)$
b3	$(0, -3)$
b4	$(-3, -3)$
b5	$(-3, 0)$
b6	$(-3, 3)$
b7	(0, 3)
b8	(3, 3)
$\xi < 1$ ($\xi = 0.3$)	
c1	(3, 0)
c2	$(0, -3)$
c3	$(-3, 0)$
c4	(0, 3)
c5	(3, 3)

New Hysteretic Damping Model

Table 3 lists all initial states $(x_0, \dot{x}_0)$ for the new hysteretic damping. In the case of $\eta > 1$ ($\eta = 1.5$), Fig. 7(a) shows that one part of trajectories yields the hyperbolic curves in the second and fourth quadrants, and the other parts yields the elliptical curves in the first

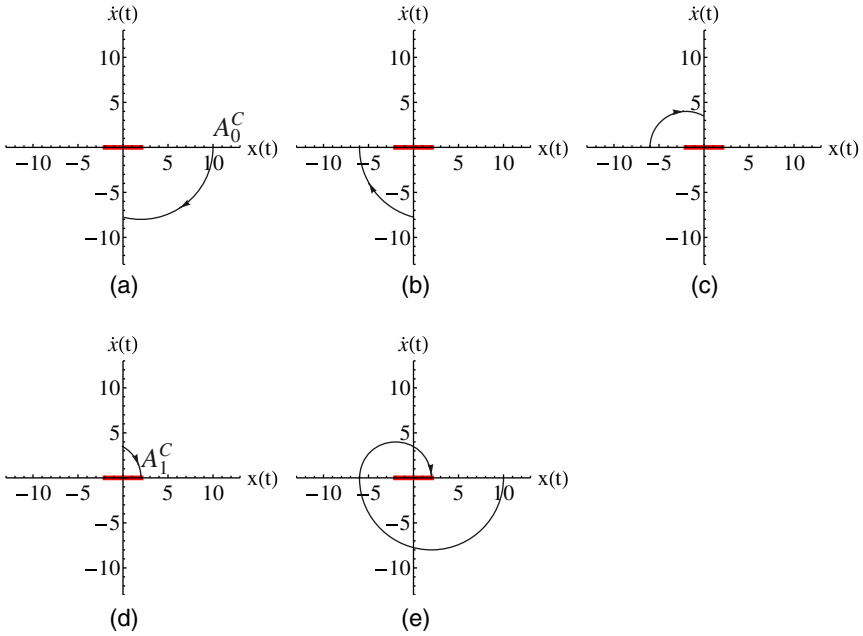

Fig. 5. Trajectories of the phase plane for the Coulomb damping model: (a) Quadrant IV; (b) Quadrant III; (c) Quadrant II; (d) Quadrant I; and (e) the total solution for $a = 2$.

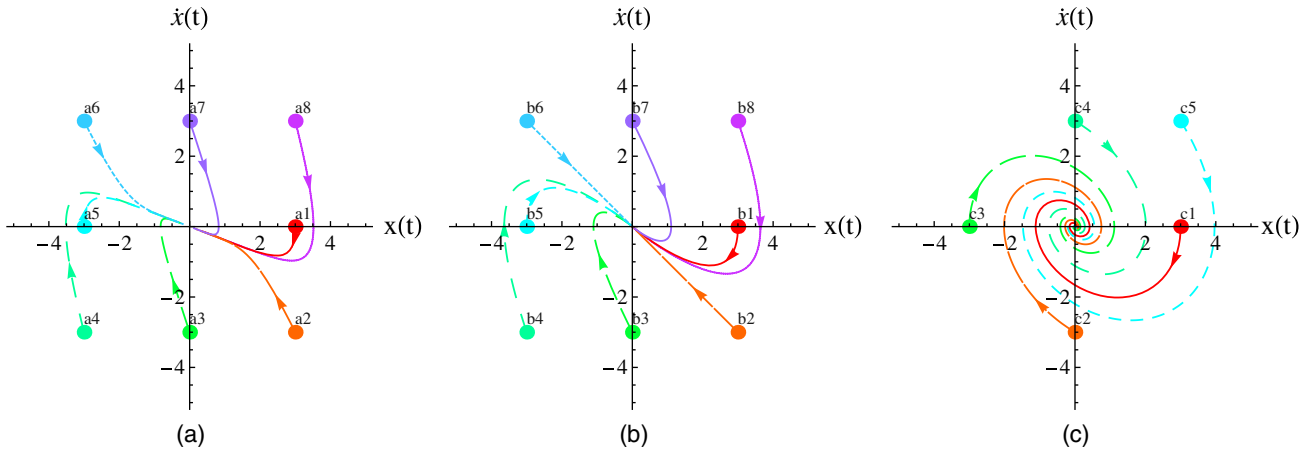

Fig. 6. Trajectories of the phase plane with various initial states for the different damping coefficient (ξ) of viscous damping model: (a) overdamping ($\xi = 1.5$); (b) critical damping ($\xi = 1$); and (c) underdamping ($\xi = 0.3$).

Table 3. Initial state $(x_0, \dot{x}_0)$ of new hysteretic damping

Case number	$(x_0, \dot{x}_0)$
$\eta > 1$ ($\eta = 1.5$)	
d1	$(-5, 4.95)$
d2	$(-5, 4.24)$
d3	$(-5, 3.54)$
d4	$(-5, 3.38)$
d5	$(-5, 3.18)$
d6	$(5, -3.18)$
d7	$(5, -3.38)$
d8	$(5, -3.54)$
d9	$(5, -4.24)$
d10	$(5, -4.95)$
$\eta = 1$	
e1	$(-5, 4.95)$
e2	$(-5, 4.24)$
e3	$(-5, 3.54)$
e4	$(-5, 2.83)$
e5	$(-5, 2.12)$
e6	$(5, -2.12)$
e7	$(5, -2.83)$
e8	$(5, -3.54)$
e9	$(5, -4.24)$
e10	$(5, -4.95)$
$\eta < 1$ ($\eta = 0.3$)	
f1	(3, 0)
f2	(0, 3)
f3	(3, 3)

and third quadrants. In particular, trajectories can be a straight line if an initial state locates on the asymptotic line of the hyperbola in the second and fourth quadrants. The function for asymptotic line of hyperbola is

$$\frac{\dot{x}(t)}{\omega_{h2}} = -x(t) \tag{32}$$

In case of $\eta = 1$, Fig. 7(b) shows that the trajectories consist of a horizontal line in the second and fourth quadrants and a quarter of ellipse in the first and third quadrants. Two cases both yield a permanent deformation of the frozen point on the $x(t)$ axis. In the case of $\eta < 1$ ($\eta = 0.3$), Fig. 7(c) shows the trajectories combining four quarter-ellipses in the phase plane. The final point of trajectory finally rests on the origin.

As mentioned previously, the models of viscous damping and the hysteretic damping both oscillate when the damping coefficients ξ and η are both less than one. The trajectories are smooth shrinking spirals in the phase plane. Two models rest at the origin in the phase plane as time increases to infinity. For the new hysteretic damping, we have stiffer spring $k(1 + \eta)$ in the first and third quadrants and softer spring $k(1 - \eta)$ in the second and fourth quadrants.

Although Crandall (1995) criticized that the new hysteretic damping model is not fully equivalent to the original one, we focus on how to capture the same physical behavior between the viscous damping model and new hysteretic damping model. It is interesting to find that two different damping models may have the same

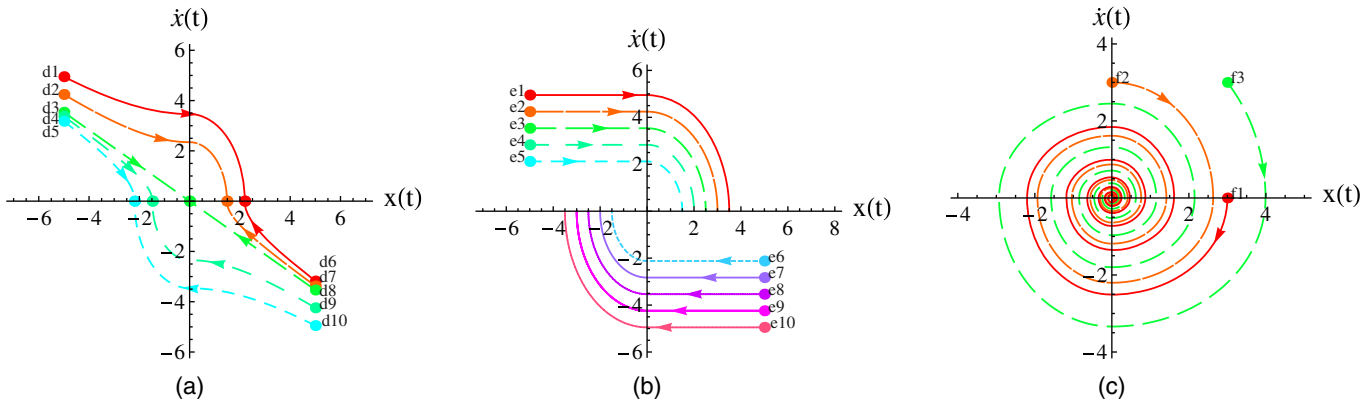

Fig. 7. Trajectories of the phase plane with various initial states for the different loss factor (η) of a new hysteretic damping model: (a) $\eta > 1$ ($\eta = 1.5$); (b) $\eta = 1$; and (c) $\eta < 1$ ($\eta = 0.3$).

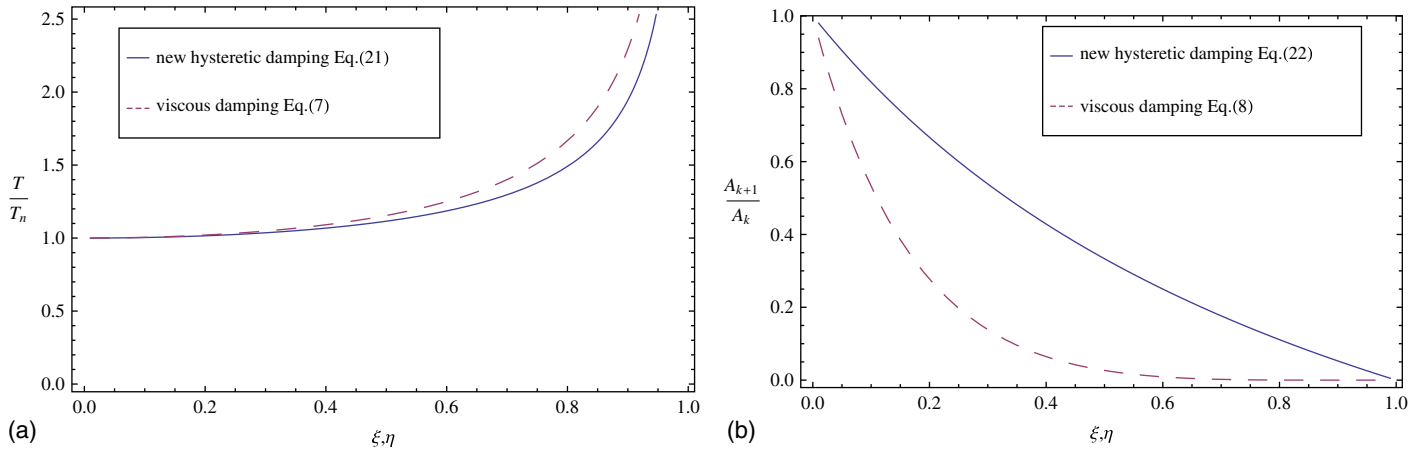

Fig. 8. Damping period and ratio of amplitude decay for viscous and new hysteretic damping models: (a) damping period versus ξ and η; and (b) ratio of amplitude decay versus ξ and η.

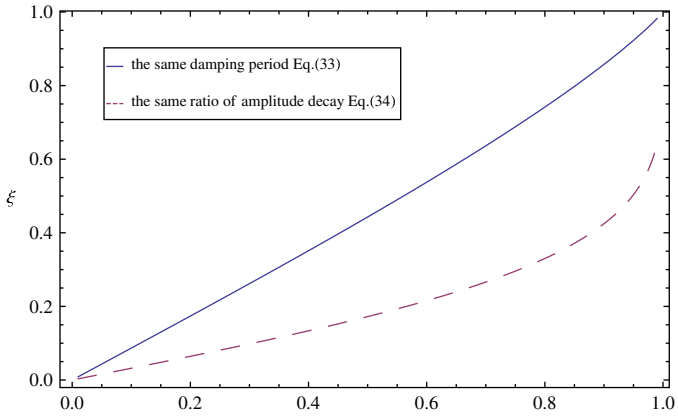

Fig. 9. Relationships between ξ and η under the conditions of the same damping period and the same ratio of amplitude decay.

damping period or the same ratio of amplitude decay in the special situation. The corresponding relationships between viscous damping and new hysteretic damping are

$$\xi = \sqrt{1 - \left(\frac{2\sqrt{1-\eta^2}}{\sqrt{1+\eta}+\sqrt{1-\eta}}\right)^2} \quad \text{for the same damping period} \tag{33}$$

$$\xi = \sqrt{\frac{\left(\ln\left(\frac{1-\eta}{1+\eta}\right)\right)^2}{\left(\ln\left(\frac{1-\eta}{1+\eta}\right)\right)^2 + 4\pi^2}} \quad \text{for the same ratio of amplitude decay} \tag{34}$$

Fig. 8(a) shows the damping period versus ξ or η, while Fig. 8(b) shows the ratio of amplitude decay versus ξ or η. It is found that the ratio of amplitude decay differs a lot between viscous and new hysteretic cases, while the damped period of the two models is closer to each other. To demonstrate this finding, Fig. 9 shows the relation between ξ and η to yield the same damped period and the same ratio of amplitude decay. For the case of the same damped period, the relation of ξ and η shows like a straight line ($\xi \approx \eta$), while it is not for the same ratio of amplitude decay. Figs. 10(a and b) show the displacement response for the same damping period with $\eta = 0.5$ and $\xi = 0.442891$ when the initial states of two damping models $(x_0, \dot{x}_0)$ are (5, 0). Figs. 11(a and b) show the displacement response for the same ratio of amplitude decay with $\eta = 0.5$ and $\xi = 0.172237$ when the initial states of two damping models $(x_0, \dot{x}_0)$ are (5, 0).

Coulomb Damping Model

The friction parameter a is 2. Table 4 shows five initial states $(x_0, \dot{x}_0)$ for the Coulomb damping model. Fig. 12 shows the trajectories in the phase plane. It is constructed by combining two half

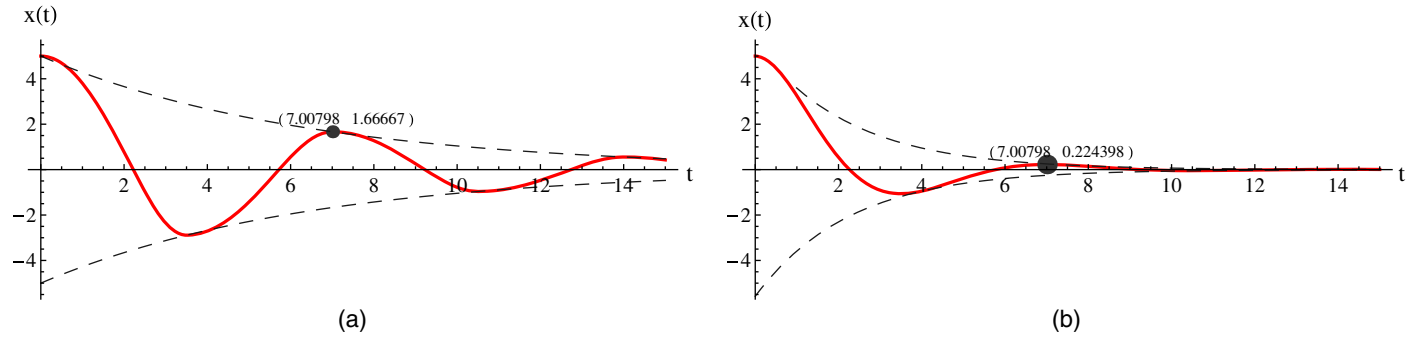

Fig. 10. Displacement history with the same damping period for two damping models: (a) new hysteretic damping ($\eta = 0.5$); and (b) viscous damping ($\xi = 0.442891$).

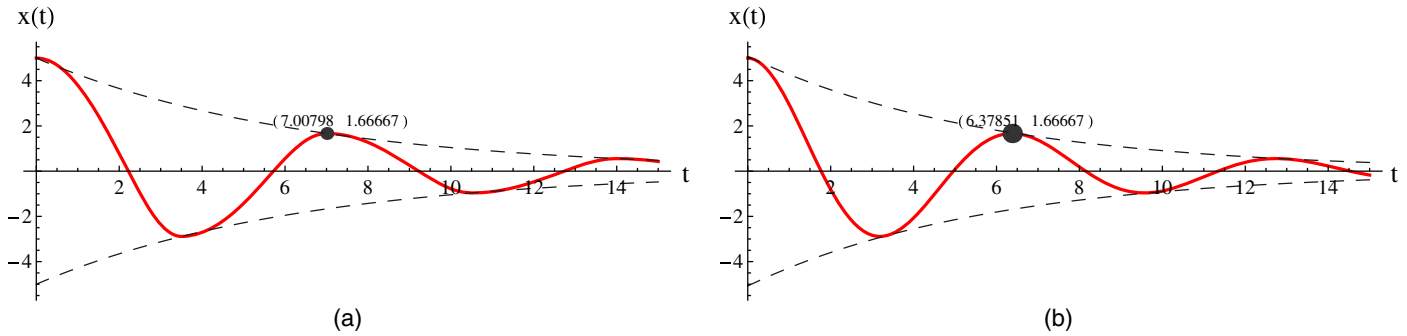

Fig. 11. Displacement history with the same ratio of amplitude decay for two damping models: (a) new hysteretic damping ($\eta = 0.5$); and (b) viscous damping ($\xi = 0.172237$).

Table 4. Initial state $(x_0, \dot{x}_0)$ of Coulomb damping ($a = 2$)

Case number	$(x_0, \dot{x}_0)$
g1	(3, 0)
g2	(9, 0)
g3	(0, 3)
g4	(0, 9)
g5	(9, 9)

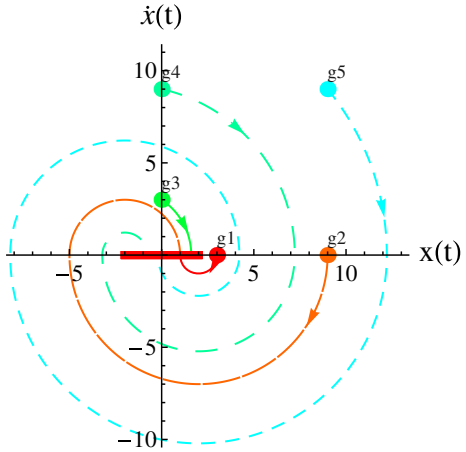

Fig. 12. Trajectories of the phase plane with various initial states for the Coulomb damping model, $a = 2$.

Table 5. Summary of three damping models

Characteristic	Viscous damping	New hysteretic damping	Coulomb damping
Exact solution	Eqs. (3)–(5)	Eqs. (17)–(19)	Eq. (27)
Effective frequency	Eq. (6)	Eq. (20)	ω_n
Damping period	Eq. (7)	Eq. (21)	Eq. (28)
Amplitude decay	Eq. (8)	Eq. (22)	Eq. (29)

elliptical curves. Owing to the friction force, the size of half elliptical curves becomes smaller and smaller. The dead zone is marked.

For detail, all the animations on the website are provided by MSV Lab. in NTOU (2017). Finally, exact solutions of three damping models are summarized in Table 5. In addition, all numerical results such as the behavior of the amplitude decay can be for references to choose the proper damping model in the experiment.

Conclusions

In this paper, we revisited three damping models in the time domain. From the academic point of view, we derive the exact solution for the new hysteresis damping in the cases of $\eta = 1$ and $\eta > 1$. The value of the new hysteretic damping loss factor $\eta = 1$ is the critical value that can be used to determine whether the hysteretic damping system oscillates or not. In other words, the value of $\eta = 1$ can be an index that we judge the mechanical system whether the permanent deformation occurs or not. It is interesting that permanent deformation do not occur in the case of $\eta > 1$ while the initial condition is given on the asymptotic line of the hyperbola in the phase plane. Also, the relation between the viscous coefficient and hysteretic parameter in the same damping period and the same ratio of amplitude decay conditions is discussed. The general solutions of three damping models for any arbitrary initial states were analytically derived by using the phase plane method. Not only trajectories of the phase plane but also mechanical systems were shown in animations by using the Mathematica software. From the educational point of view, students may easily understand the physical phenomenon and the mechanical system of three damping models through animations. In addition, students can choose the proper damping model when the experimental data of decay behavior is obtained. Therefore, a black box becomes apparent to be three damping models by more physical meaning.

References

Beards, C. 1995. *Engineering vibration analysis with application to control systems*, 29–42. 1st ed. London, UK: Edward Arnold.

Beucke, K. E., and J. M. Kelly. 1985. "Equivalent linearizations for practical hysteretic systems." *Int. J. Non-Linear Mech.* 20 (4): 211–238. https://doi.org/10.1016/0020-7462(85)90031-9.

Caughey, T. K., and A. Vijayaraghavan. 1970. "Free and forced oscillations of a dynamic system with linear hysteretic damping." *Int. J. Non-Linear Mech.* 5 (3): 533–555. https://doi.org/10.1016/0020-7462(70)90015-6.

Chen, J. T., K. S. Chou, and S. K. Kao. 2009. "One-dimensional wave animation using Mathematica." *Comput. Appl. Eng. Educ.* 17 (3): 323–339. https://doi.org/10.1002/cae.20224.

Chen, J. T., and D. W. You. 1997. "Hysteretic damping revisited." *Adv. Eng. Software* 28 (3): 165–171. https://doi.org/10.1016/S0965-9978(96)00052-X.

Chen, J. T., and D. W. You. 1999. "An integral-differential equation approach for the free vibration SDOF system with hysteretic damping." *Adv. Eng. Software* 30 (1): 43–48. https://doi.org/10.1016/S0965-9978(98)00061-1.

Chen, L. Y., J. T. Chen, C. H. Chen, and H. K. Hong. 1994a. "Free vibration of a SDOF system with hysteretic damping." *Mech. Res. Commun.* 21 (6): 599–604. https://doi.org/10.1016/0093-6413(94)90023-X.

Chen, L. Y., J. T. Chen, C. H. Chen, and H. K. Hong. 1994b. "The time-domain solution of a hysteretic damping system in the phase plane." In *Proc., 2nd Annual Conf. of Vibration and Acoustics*, 119–128. Taipei, Taiwan: Chinese Society of Sound and Vibration.

Clough, R. W., and J. Penzien. 1975. *Dynamics of structures*. 1st ed. New York, NY: McGraw-Hill.

Crandall, S. H. 1995. "A new hysteretic damping model?" *Mech. Res. Commun.* 22 (2): 201–202. https://doi.org/10.1016/S0093-6413(99)80001-9.

Gaul, L. 1989. "Structural damping in frequency and time domain." In *Proc., 7th Int. Modal Analysis Conf.*, 177–184. Schenectady, NY: Union College.

Gaul, L., S. Bohlen, and S. Kempfle. 1985. "Transient and forced oscillation of systems with constant hysteretic damping." *Mech. Res. Commun.* 12 (4): 187–201. https://doi.org/10.1016/0093-6413(85)90057-6.

Inaudi, J., and J. Kelly. 1995. "Linear hysteretic damping and the Hilbert transform." *J. Eng. Mech.* 121 (5): 626–632. https://doi.org/10.1061/(ASCE)0733-9399(1995)121:5(626).

Inaudi, J., and N. Makris. 1996. "Time-domain analysis of linear hysteretic damping." *Earthquake Eng. Struct. Dyn.* 25 (6): 529–545. https://doi.org/10.1002/(SICI)1096-9845(199606)25:6<529::AID-EQE549>3.0.CO;2-P.

Kuo, S. R., and J. T. Chen. 1999. "Forced vibration of a SDOF system with a new hysteretic damping subjected to harmonic loading." *Int. J. Appl. Mech.* 1 (4): 411–438.

Makris, N. 1997. "Causal hysteretic element." *J. Eng. Mech.* 123 (11): 1209–1214. https://doi.org/10.1061/(ASCE)0733-9399(1997)123:11(1209).

Makris, N., J. Inaudi, and J. Kelly. 1996. "Macroscopic models with complex coefficients and causality." *J. Eng. Mech.* 122 (6): 566–573. https://doi.org/10.1061/(ASCE)0733-9399(1996)122:6(566).

Meirovitch, L. 1986. *Elements of vibration analysis*. 2nd ed. New York, NY: McGraw-Hill.

Nashif, A. D., D. I. G. Jones, and J. P. Henderson. 1985. *Vibration damping*. 1st ed. New York, NY: Wiley.

NTOU. 2017. "Animation of three damping models (2017)." Accessed August 5, 2017. http://goo.gl/RvDLx3.

Sun, C. T., and Y. P. Lu. 1994. *Vibration damping of structural elements*. 1st ed. Englewood Cliffs, NJ: Prentice Hall.

Zhuravlev, V. P. 2013. "On the history of the dry friction law." *Mech. Solids* 48 (4): 364–369. https://doi.org/10.3103/S002565441304002X.